J Solution Chem (2018) 47:595–610
https://doi.org/10.1007/s10953-018-0742-z

Experimental Determination of Solubilities of Brucite [$Mg(OH)_2$(cr)] in Na_2SO_4 Solutions with Borate to High Ionic Strengths: Interactions of $MgB(OH)_4^+$ with Na_2SO_4

Yongliang Xiong[1] · **Leslie Kirkes**[1] · **Terry Westfall**[1]

Received: 3 February 2017 / Accepted: 20 November 2017 / Published online: 18 April 2018
© Springer Science+Business Media, LLC, part of Springer Nature 2018

Abstract In this work, a solubility study on brucite [$Mg(OH)_2$(cr)] in Na_2SO_4 solutions ranging from 0.01 to 1.8 mol·kg^{-1}, with 0.001 mol·kg^{-1} borate, has been conducted at 22.5 °C. Based on the solubility data, the Pitzer interaction parameters for $MgB(OH)_4^+ - SO_4^{2-}$ and $MgB(OH)_4^+ - Na^+$ along with the formation constant for $MgSO_4$(aq) are evaluated using the Pitzer model. The formation constant ($\log_{10}\beta_1^0 = 2.38 \pm 0.08$) for $MgSO_4$(aq) at 25 °C and infinite dilution obtained in this study is in excellent agreement with the literature values. The experimental data on the solubility of gypsum ($CaSO_4{\cdot}2H_2O$), at 25 °C, in aqueous solutions of $MgSO_4$ with ionic strengths up to $\sim$ 11 mol·kg^{-1} were analyzed using models with and without considering the $MgSO_4$(aq) species. The model incorporating $MgSO_4$(aq) fits better to the experimental data than the model without $MgSO_4$(aq), especially in the ionic strength range beyond $\sim$ 4 mol·kg^{-1}, demonstrating the need for incorporation of $MgSO_4$(aq) into the model to improve the accuracy.

Keywords Nuclear waste management · Pitzer model · Corrosion of Mg-based alloys · Gypsum · Degradation of cement

1 Introduction

An accurate knowledge of solubilities of brucite ($Mg(OH)_2$) in sulfate solutions is important to numerous fields. In the field of nuclear waste management, brucite has become important to waste isolation projects owing to its use as engineered barriers for nuclear waste repositories. Crystalline MgO, which hydrates rapidly to brucite [1], is the only engineered barrier certified by the US Environmental Protection Agency (EPA) for

✉ Yongliang Xiong
yxiong@sandia.gov

[1] Sandia National Laboratories (SNL), Carlsbad Programs Group, 4100 National Parks Highway, Carlsbad, NM 88220, USA

the Waste Isolation Pilot Plant (WIPP) located near Carlsbad, New Mexico, USA (e.g., [1, 2]). The WIPP is in a bedded salt formation. An $Mg(OH)_2$-based engineered barrier is also proposed for the German Asse salt mine repository [3]. Sulfate is a major species in some natural brines associated with salt formations. For instance, the sulfate concentrations in the two WIPP brines important to the performance assessment (PA), i.e., Generic Weep Brine (GWB) and U.S. Energy Research and Development Administration Well 6 (ERDA-6) are 0.203 and 0.187 $mol{\cdot}kg^{-1}$, respectively [1]. The sulfate concentrations in the Q-brine at the Asse are 0.2 $mol{\cdot}kg^{-1}$ [4]. In addition, the borate concentrations in the WIPP brines GWB and ERDA-6, are 0.178 $mol{\cdot}kg^{-1}$ (or 0.0445 $mol{\cdot}kg^{-1}$ if it is expressed as $B_4O_7^{2-}$) and 0.0704 $mol{\cdot}kg^{-1}$ (or 0.0176 $mol{\cdot}kg^{-1}$ if it is expressed as $B_4O_7^{2-}$), respectively. Therefore, accurate knowledge about the solubility of brucite in sulfate solutions is important to the performance of the engineered barrier. Finally, in the low and intermediate level radioactive sulfate liquid wastes (LLW and ILW) in Spain, the associated solutions are very rich in SO_4^{2-}, up to 2.2 $mol{\cdot}kg^{-1}$ [5]. Cements are proposed to be the waste form for such LLW and ILW [5]. When portlandite [$Ca(OH)_2$(cr)], the major component of cements with MgO being a minor constituent, is transformed into gypsum ($CaSO_4{\cdot}2H_2O$) in such sulfate-rich environments, the solubility of gypsum in sulfate solutions in the presence of Mg(II) will be important to the performance of cement waste form.

In the field of construction, Portland cement pastes are subject to $MgSO_4$ solutions attack (e.g., [6–8]). When such an attack occurs, brucite forms on the surface almost immediately after cements are in contact with the solution [8]. As the molar volume of $Mg(OH)_2$ is higher than that of portlandite [$Ca(OH)_2$] [9], the amounts of brucite formed have direct impact on the deterioration of cements.

In the field of metallurgy and corrosion science, magnesium-based alloys are widely used in various industries. In addition, magnesium is also used as magnesium-rich primers to protect aluminum-based alloys (e.g., [10]). When magnesium-based alloys such as AZ91D and AZ30, and magnesium-rich primers are corroded in sulfate solutions, brucite forms (e.g., [11–15]). Therefore, accurate knowledge of brucite solubility in sulfate solutions will provide a better understanding of corrosion behavior of magnesium-based alloys and magnesium-rich primers, and hence enable researchers to predict the performance of these alloys and primers when they are subject to corrosion in sulfate solutions.

As accurate knowledge of brucite solubility in sulfate-bearing solutions will impact a wide range of fields, we investigate solubilities of brucite in Na_2SO_4 solutions in the presence of borate, with a wide range of ionic strengths up to 5.4 $mol{\cdot}kg^{-1}$ in this work. We performed long-term solubility measurements in our work, approaching equilibrium from the direction of undersaturation in Na_2SO_4 solutions at the following concentrations: 0.01, 0.1, 0.5, 1.0, 1.5 and 1.8 $mol{\cdot}kg^{-1}$, with a borate concentration of 0.001 $mol{\cdot}kg^{-1}$. The objective of this work is to investigate the specific interactions of $MgB(OH)_4^+$ with a Na_2SO_4 medium based on the solubility of brucite in Na_2SO_4 solutions in the presence of borate. In previous studies ([16], and references therein), the specific interactions of brucite with a NaCl medium have been investigated. Based on the experimental data from the current work, we develop a Pitzer model to describe solubilities of brucite in Na_2SO_4 solutions in the presence of borate, to high ionic strengths.

2 Experimental Methodology

All materials (Na_2SO_4, $Mg(OH)_2$, and H_3BO_3) used in this study are reagent grade from Fisher Scientific. The purity of Na_2SO_4 was 99.99%. The purity of $Mg(OH)_2$ and H_3BO_3 was 99.9%. Deionized (DI) water with 18.3 MΩ was produced by a Barnstead NANOpure Water System from Thermo Scientific. Degassed DI water was used for preparation of all starting solutions. The degassed DI water was obtained by bubbling high purity argon gas (purity 99.996%) from AIR GAS, Inc., through DI water for at least one hour, following a procedure similar to that described by Wood et al. [17]. Starting solutions were prepared such that the equilibrium solubility was approached from under-saturation with respect to brucite. The experimental duration for reaching equilibrium with brucite has been established before in NaCl solutions from both under- and super-saturation [16].

Solubility experiments approaching equilibrium from the direction of undersaturation were conducted at six concentrations of Na_2SO_4, i.e., 0.010, 0.10, 0.50, 1.0, 1.5, and 1.8 mol·kg^{-1} Na_2SO_4 with 0.001 mol·kg^{-1} H_3BO_3. At each concentration of Na_2SO_4, experiments were set-up in duplicate.

All experiments were conducted at room temperature (22.5 ± 0.5 °C). For each of the experiments undersaturated with respect to brucite, 5 grams of $Mg(OH)_2$(cr) were placed into a 150 mL polyethylene bottles containing 100 mL of a supporting solution (a Na_2SO_4 solution with 0.001 mol·kg^{-1} H_3BO_3).

The pH readings were measured with an Orion-Ross combination pH glass electrode, coupled with an Orion Research EA 940 pH meter. Before each measurement, the pH meter was calibrated with three pH buffers (pH 4, pH 7, and pH 10). In solutions with an ionic strength higher than 0.10 mol·kg^{-1}, negative logarithms of hydrogen-ion concentrations on molar scale (pcH) were determined from pH readings by using correction factors for Na_2SO_4 solutions determined before [18], which were re-analyzed [19]. Based on the equation in Xiong et al. [20], pcHs are converted to negative logarithms of hydrogen-ion concentrations on the molal scale (pH_m).

As described above, therefore, the pH scale adopted by this work was a concentration scale. The concentrations of hydrogen-ion were determined based on the correction factors for converting pH readings to pcH, and then pH_m.

Solution samples were periodically withdrawn from experimental runs. Before solution samples were taken, pH readings of experimental runs were measured. The sample size was usually 3 mL. After a solution sample was withdrawn from an experiment and filtered with a 0.2 μm syringe filter, the filtered solution was then weighed, acidified with 0.5 mL of concentrated TraceMetal® grade HNO_3 from Fisher Scientific, and finally diluted to a volume of 10 mL with DI water. If subsequent dilutions were needed, aliquots were taken from the first dilution samples for the second dilution, and aliquots of the second dilution were then taken for further dilution.

The chemical analyses of solutions were performed with a Perkin Elmer dual-view inductively coupled plasma-atomic emission spectrometer (ICP-AES) (Perkin Elmer DV 3300). Calibration blanks and standards were precisely matched with experimental matrices. The linear correlation coefficients of calibration curves in all measurements were better than 0.9995. The analytical precision for ICP-AES was better than 1.00% in terms of the relative standard deviation (RSD) based on replicate analyses.

Solid phase identification was performed by using a Bruker AXS, Inc., D8 Advance X-ray diffractometer (XRD) with a Sol-X detector. XRD patterns were collected using CuKα radiation at a scanning rate of 1.33°/min for a 2θ range of 10–90°. There was no

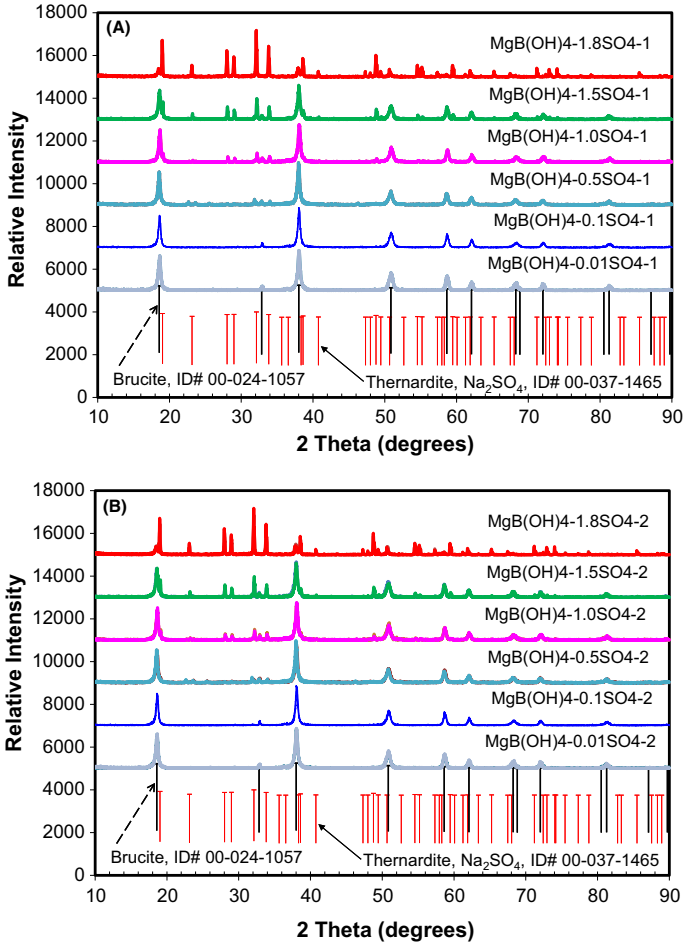

Fig. 1 XRD patterns for the experiments conducted in this study after the experimental runs. **a** XRD patterns for all experiments with Replicate 1. **b** XRD patterns for all experiments with Replicate 2. The XRD standards for brucite [$Mg(OH)_2$(cr)] (in black) and thernardite [Na_2SO_4(cr)] (in red) are from PDF-4 + 2016 (Software Version 4.16.04, Database Version 4.1605) of the International Center for Diffraction Data (ICDD). Notice that the peaks for thernardite appeared in the XRD patterns for the experimental runs in 0.5, 1.0, 1.5 and 1.8 mol·kg^{-1} Na_2SO_4, because thernardite crystallized from the residual Na_2SO_4 solutions when the samples were dried (Color figure online)

phase change as indicated by Fig. 1a, b. The presence of thernardite [Na_2SO_4(cr)] in the XRD patterns for the experimental runs in 0.5, 1.0, 1.5 and 1.8 mol·kg^{-1} Na_2SO_4 (Fig. 1a, b) was due to the fact that thernardite crystallized from the residual Na_2SO_4 solutions when the samples were dried for XRD analyses.

3 Experimental Results

In all of the experiments, the solubility-controlling phase is brucite (Fig. 1a, b). The experimental results including molalities of magnesium and pH_m for the solubility of brucite in aqueous solutions of sodium sulfate containing 0.001 mol·kg^{-1} H_3BO_3, are tabulated in Table 1. The durations of the experiments were up to 383 days. The experimental time was long enough to ensure the attainment of equilibrium. Xiong [16], has demonstrated, from both undersaturation and supersaturation experiments in NaCl and $MgCl_2$ solutions, that the duration of experimental time for attainment of equilibrium is $\sim$ 83 days (i.e., $\sim$ 2000 h).

In Fig. 2 are shown the equilibrium total magnesium molalities [i.e., ΣMg(II)] (on a logarithmic scale) as a function of experimental time. Figure 2 shows the attainment of equilibrium, which is illustrated by the constant molalities of magnesium as a function of experimental time, especially for the experiments at lower ionic strengths (i.e., 0.01 and 0.1 mol·kg^{-1} Na_2SO_4). However, there are some scatters in magnesium molality for the experiments at higher ionic strengths (e.g., 1.5, 1.8 mol·kg^{-1} Na_2SO_4) owing to slight variations in pH_m (Fig. 3).

In Fig. 3, pH_m as a function of experimental time is displayed. Figure 3 shows that the pH_m generally varies from $\sim$ 10.1 to $\sim$ 10.3, which is within the usually combined uncertainties from the procedure and the instrument. Of note, the procedural uncertainty in measuring pH above pH 10 is $\sim$ 0.15 [21]. The pH_m almost remains constant in the experiments in lower ionic strength solutions (i.e., 0.01 and 0.1 mol·kg^{-1} Na_2SO_4) (Fig. 3). There are relatively higher variations in pH_m in the experiments in higher ionic strength solutions (e.g., 1.8 mol·kg^{-1} Na_2SO_4), contributing to the scatters in molality of magnesium for the respective experiments, as solubilities of brucite are pH_m dependent, as suggested by the following reaction,

$$Mg(OH)_2(cr) + 2H^+ \rightleftharpoons Mg^{2+} + 2H_2O(l) \quad (1)$$

In Reaction (1), the equilibrium quotient can be written as

$$Q = \frac{m_{\Sigma Mg(II)}}{(m_{H^+})^2} \quad (2)$$

Reaction (1) implies that when m_{H^+} changes, magnesium concentrations will correspondingly change.

In Fig. 4, $\log_{10} \frac{m_{\Sigma Mg(II)}}{(m_{H^+})^2}$ is plotted against the experimental time. It can be seen that the variations in $\log_{10} \frac{m_{\Sigma Mg(II)}}{(m_{H^+})^2}$ versus experimental time seem to be statistically indistinguishable, which is consistent with what was observed in the literature. The experimental data for short durations from McGee and Hostetler [22] in pure water at 25 °C from the direction of undersaturation are also plotted in Fig. 4. The longest experimental run in their experiments lasted for $\sim$ 13 days (316 h). In the enlarged insert for their data in Fig. 4, there are variations in $\log_{10} \frac{m_{\Sigma Mg(II)}}{(m_{H^+})^2}$ versus experimental time, but they are also statistically indistinguishable. In Fig. 4, the experimental data from [16] approaching equilibrium from the direction of supersaturation started with a 0.1 mol·kg^{-1} $MgCl_2$ solution are also plotted. The duration for that experimental run from [16], which lasted for up to 1514 days, was much longer than that in this work. After attainment of equilibrium at $\sim$ 83 days for that experimental run from supersaturation [16], Fig. 4 shows that there are statistically

Table 1 Experimental results concerning solubility of brucite ($Mg(OH)_2$(cr)), as total magnesium molality, in Na_2SO_4 solutions with 0.001 mol·kg^{-1} H_3BO_3, at 22.5 ± 0.5 °C

Experimental number	Supporting medium, $m_{Na_2SO_4}$ (mol·kg^{-1})	Experiment time (days)	pH_m[a]	Solubility of brucite, $m_{Mg,total}$ (mol·kg^{-1})
$MgB(OH)_4$–0.01SO_4-1	0.010	233	10.13	2.10×10^{-3}
$MgB(OH)_4$–0.01SO_4-2	0.010	233	10.14	2.11×10^{-3}
$MgB(OH)_4$–0.1SO_4-1	0.10	233	10.20	2.87×10^{-3}
$MgB(OH)_4$–0.1SO_4-2	0.10	233	10.23	2.80×10^{-3}
$MgB(OH)_4$–0.5SO_4-1	0.50	233	10.17	3.65×10^{-3}
$MgB(OH)_4$–0.5SO_4-2	0.50	233	10.15	3.60×10^{-3}
$MgB(OH)_4$–1.0SO_4-1	1.0	233	10.12	3.87×10^{-3}
$MgB(OH)_4$–1.0SO_4-2	1.0	233	10.12	3.88×10^{-3}
$MgB(OH)_4$–1.5SO_4-1	1.5	233	10.16	4.19×10^{-3}
$MgB(OH)_4$–1.5SO_4-2	1.5	233	10.16	2.80×10^{-3}
$MgB(OH)_4$–1.8SO_4-1	1.8	233	10.21	4.56×10^{-3}
$MgB(OH)_4$–1.8SO_4-2	1.8	233	10.21	4.67×10^{-3}
$MgB(OH)_4$–0.01SO_4-1	0.010	285	10.17	2.01×10^{-3}
$MgB(OH)_4$–0.01SO_4-2	0.010	285	10.18	2.01×10^{-3}
$MgB(OH)_4$–0.1SO_4-1	0.10	285	10.28	2.72×10^{-3}
$MgB(OH)_4$–0.1SO_4-2	0.10	285	10.29	2.72×10^{-3}
$MgB(OH)_4$–0.5SO_4-1	0.50	285	10.24	3.47×10^{-3}
$MgB(OH)_4$–0.5SO_4-2	0.50	285	10.25	3.43×10^{-3}
$MgB(OH)_4$–1.0SO_4-1	1.0	285	10.19	3.71×10^{-3}
$MgB(OH)_4$–1.0SO_4-2	1.0	285	10.20	3.68×10^{-3}
$MgB(OH)_4$–1.5SO_4-1	1.5	285	10.24	3.91×10^{-3}
$MgB(OH)_4$–1.5SO_4-2	1.5	285	10.24	3.87×10^{-3}
$MgB(OH)_4$–1.8SO_4-1	1.8	285	10.30	4.03×10^{-3}
$MgB(OH)_4$–1.8SO_4-2	1.8	285	10.31	4.22×10^{-3}
$MgB(OH)_4$–0.01SO_4-1	0.010	335	10.16	1.93×10^{-3}
$MgB(OH)_4$–0.01SO_4-2	0.010	335	10.18	1.95×10^{-3}
$MgB(OH)_4$–0.1SO_4-1	0.10	335	10.25	2.72×10^{-3}
$MgB(OH)_4$–0.1SO_4-2	0.10	335	10.25	2.72×10^{-3}
$MgB(OH)_4$–0.5SO_4-1	0.50	335	10.17	3.72×10^{-3}
$MgB(OH)_4$–0.5SO_4-2	0.50	335	10.17	3.68×10^{-3}
$MgB(OH)_4$–1.0SO_4-1	1.0	335	10.09	4.19×10^{-3}
$MgB(OH)_4$–1.0SO_4-2	1.0	335	10.07	4.13×10^{-3}
$MgB(OH)_4$–1.5SO_4-1	1.5	335	10.11	4.38×10^{-3}
$MgB(OH)_4$–1.5SO_4-2	1.5	335	10.08	4.39×10^{-3}
$MgB(OH)_4$–1.8SO_4-1	1.8	335	10.15	4.77×10^{-3}
$MgB(OH)_4$–1.8SO_4-2	1.8	335	10.16	4.98×10^{-3}
$MgB(OH)_4$–0.01SO_4-1	0.010	383	10.21	1.95×10^{-3}
$MgB(OH)_4$–0.01SO_4-2	0.010	383	10.22	1.99×10^{-3}
$MgB(OH)_4$–0.1SO_4-1	0.10	383	10.29	2.61×10^{-3}
$MgB(OH)_4$–0.1SO_4-2	0.10	383	10.27	2.53×10^{-3}
$MgB(OH)_4$–0.5SO_4-1	0.50	383	10.28	2.80×10^{-3}
$MgB(OH)_4$–0.5SO_4-2	0.50	383	10.22	2.86×10^{-3}

Table 1 continued

Experimental number	Supporting medium, $m_{Na_2SO_4}$ (mol·kg^{-1})	Experiment time (days)	pH_m[a]	Solubility of brucite, $m_{Mg,total}$ (mol·kg^{-1})
$MgB(OH)_4$–1.0SO_4-1	1.0	383	10.20	3.02×10^{-3}
$MgB(OH)_4$–1.0SO_4-2	1.0	383	10.21	2.99×10^{-3}
$MgB(OH)_4$–1.5SO_4-1	1.5	383	10.18	3.28×10^{-3}
$MgB(OH)_4$–1.5SO_4-2	1.5	383	10.17	3.10×10^{-3}
$MgB(OH)_4$–1.8SO_4-1	1.8	383	10.23	3.23×10^{-3}
MgB(OH)4–1.8SO_4-2	1.8	383	10.23	3.45×10^{-3}

[a]Negative logarithms of hydrogen ion concentrations on a molal scale, mol·kg^{-1}

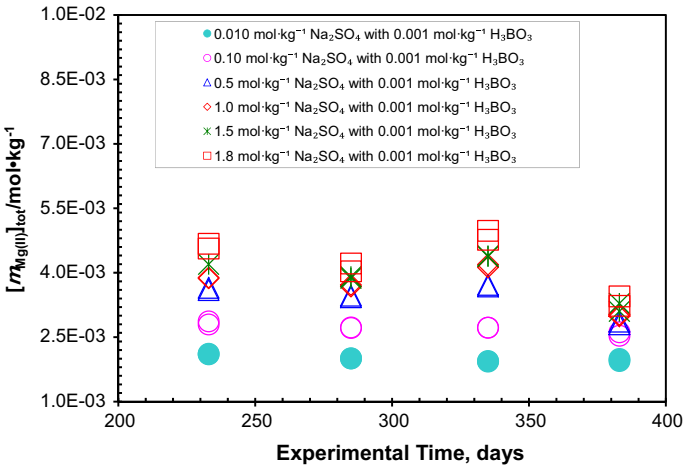

Fig. 2 A plot showing molalities of magnesium in equilibrium with brucite as a function of experimental time

indistinguishable variations in $\log_{10} \frac{m_{\Sigma Mg(II)}}{(m_{H^+})^2}$ versus experimental time, similar to those present in this study.

4 Thermodynamic Modeling

In this part, we present the thermodynamic model to describe the solubilities of brucite in Na_2SO_4 solutions in the presence of borate to high ionic strength. As the Pitzer activity coefficient model is valid to high ionic strengths, we adopt the Pitzer model as the framework.

In the modeling, the computer code, EQ3/6 Version 8.0a [23, 24], is used as the modeling platform. The EQ3/6 has been successfully utilized as the modeling platform in a number of previous studies at both ambient temperatures (e.g., [4, 25–27]) and at elevated temperatures up to 250 °C (e.g., [28–30]). The database containing all parameters necessary, including thermodynamic properties, for the modeling, is the Waste Isolation Pilot

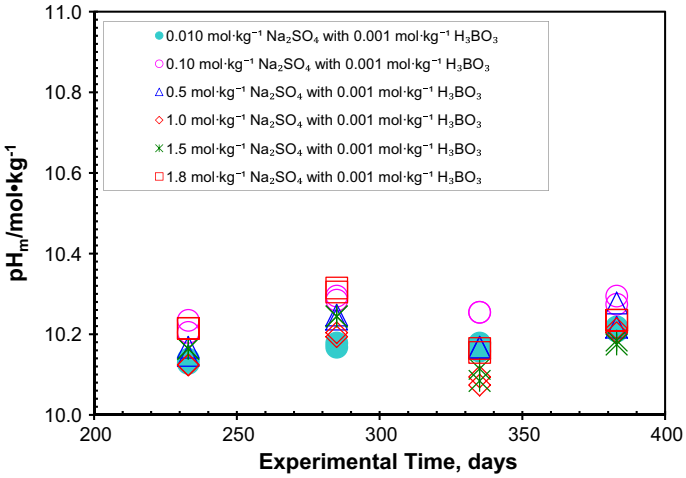

Fig. 3 A plot showing pH_m/mol·kg^{-1} in equilibrium with brucite as a function of experimental time

Plant (WIPP) thermodynamic database, DATA0.FM1 [31]. This database adopts the parameters for major ions from Harvie et al. [32].

In the model calculations, the experimental data were first used to generate EQ3/6 Version 8.0a input files. Then, a script such as a Python script was generated to call the targeted parameters, and call EQ3/6. The minimization subroutine in the script automatically compares differences between experimental values and model predicted values produced by a set of inputted parameters in each iteration. The iteration is complete when the difference is finally minimized.

In Figs. 5 and 6, solubilities of brucite as a function of ionic strengths in Na_2SO_4 solutions and as a function of pH_m, predicted by using the key parameters of the model without $MgSO_4$(aq) listed in Table 2, are shown in comparison with the experimental data. These parameters, mainly concerning the interactions with SO_4^{2-}, are from Harvie et al. [32]. Figures 5 and 6 illustrate that these parameters without $MgSO_4$(aq) do not adequately describe the experimental data.

As numerous studies suggest the existence of the complex, $MgSO_4$(aq) (e.g., [33–36]), including spectroscopic evidence [33, 36], we explicitly introduce $MgSO_4$(aq) into the model. The formation reaction for $MgSO_4$(aq) can be expressed as,

$$Mg^{2+} + SO_4^{2-} \rightleftharpoons MgSO_4(aq) \tag{3}$$

The formation constant ($\log_{10} \beta_1^0$) for Reaction (1) obtained by this study is 2.38 ± 0.08 (Table 3). Notice that the uncertainty also includes the minor corrections from 22.5 °C to the standard temperature of 25 °C. In addition, the interaction parameters for $MgB(OH)_4^+ - SO_4^{2-}$ and $MgB(OH)_4^+ - Na^+$ are also evaluated (Table 3).

The formation constant for $MgSO_4$(aq) obtained by this is in excellent agreement with the values in literature (e.g., [37–39]). For instance, Nair and Nancollas [37] obtained a value of 2.13 for $\log_{10} \beta_1^0$ based on conductivity measurement. Kester [38] calculated a value of 2.32 for $\log_{10} \beta_1^0$ based on potentiometric measurements. Noticeably, Kratsis et al. [39] determined the formation constant of $MgSO_4$(aq) via a potentiometric study with a

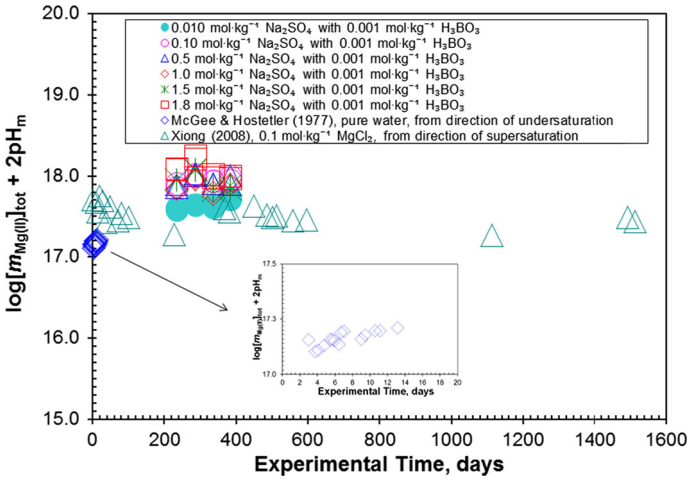

Fig. 4 A plot showing $\log_{10}\frac{m_{\Sigma Mg(II)}}{(m_{H^+})^2} = \log_{10} m_{\Sigma Mg(II)} + 2pH_m$ as a function of experimental time; note that the experimental data from McGee and Hostetler [22] was started with pure water at 25 °C

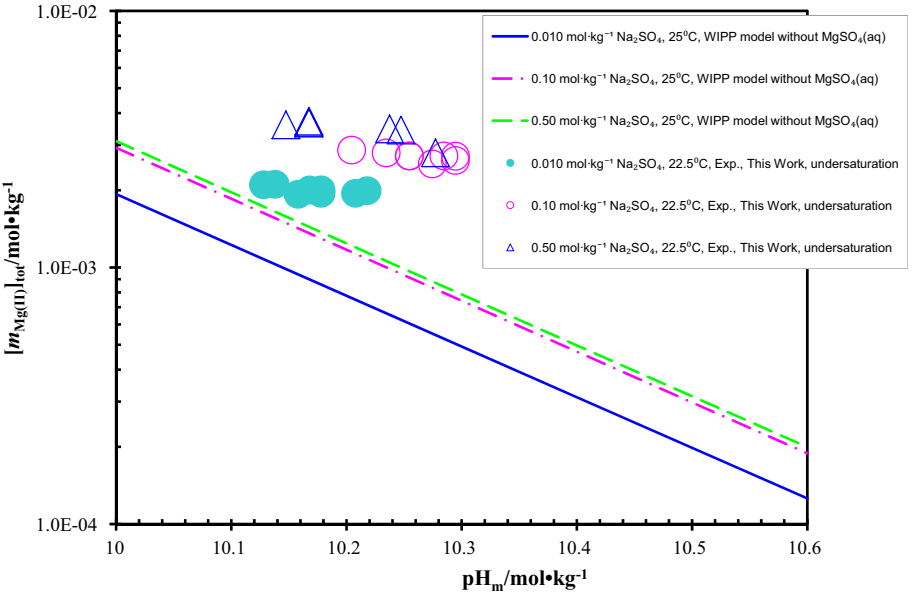

Fig. 5 A plot showing molalities of magnesium in equilibrium with brucite as a function of pH_m in Na_2SO_4 solutions ranging from 0.01 to 0.5 mol·kg^{-1}, in comparison with the predicted values using the model without $MgSO_4$(aq). The predicted values are produced using the database, DATA0.FM1, [31] (see Table 2)

magnesium ion-selective electrode. The supporting electrolyte for their work was CsCl with ionic strengths up to 6.0 mol·dm^{-3}. The $\log_{10}\beta_1^0$ obtained by Kratsis et al. [39] using the Debye–Hückel equation for extrapolation to infinite dilution is 2.38 ± 0.03.

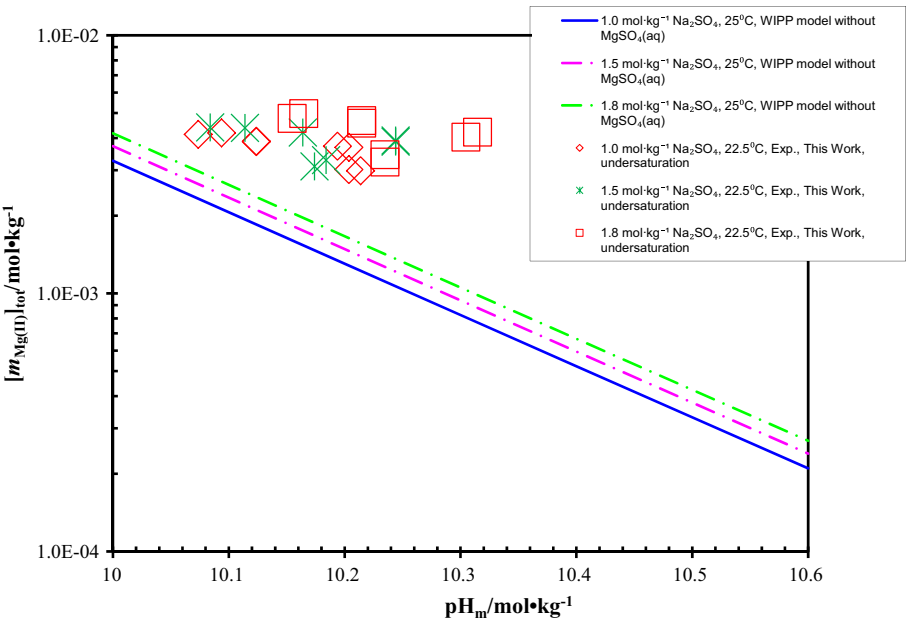

Fig. 6 A plot showing molalities of magnesium in equilibrium with brucite as a function of pH_m in Na_2SO_4 solutions ranging from 1.0 to 1.8 mol·kg^{-1}, in comparison with the predicted values using the model without $MgSO_4$(aq). The predicted values are produced utilizing the database, DATA0.FM1, [31] (see Table 2)

Table 2 Key parameters without $MgSO_4$(aq) describing solubility of brucite in Na_2SO_4 solutions with borate at 25 °C

Pitzer binary parameters				
Species, *i*	Species, *j*	$\beta^{(0)}$	$\beta^{(1)}/\beta^{(2)}$	C^{ϕ}
Mg^{2+}	SO_4^{2-}	0.221	3.343/− 37.23	0.025
Na^+	SO_4^{2-}	0.01958	1.113	0.00497
Na^+	OH^-	0.0864	0.253	0.0044

Pitzer mixing parameters				
Species, *i*	Species, *j*	Species, *k*	θ_{ij}	Ψ_{ijk}
Mg^{2+}	Na^+	SO_4^{2-}	0.07	− 0.015

Equilibrium constants at infinite dilution for dissolution reaction of brucite and dissociation reactions of $MgOH^+$ and $MgB(OH)_4^+$

Reactions	$\log_{10} K^{\circ}$
$Mg(OH)_2(cr) + 2H^+ \rightleftharpoons Mg^{2+} + 2H_2O(l)$	17.05 ± 0.20 [16]
$MgOH^+ + H^+ \rightleftharpoons Mg^{2+} + H_2O(l)$	11.8091
$MgB(OH)_4^+ \rightleftharpoons Mg^{2+} + B(OH)_4^-$	− 1.3993

Unless otherwise noted, parameters are from the WIPP thermodynamic database, DATA0.FM1 [31]

Table 3 Key parameters with $MgSO_4$(aq) describing solubility of brucite in Na_2SO_4 solutions with borate at 25 °C

Pitzer binary parameters				
Species, *i*	Species, *j*	$\beta^{(0)}$	$\beta^{(1)}/\beta^{(2)}$	C^{ϕ}
Mg^{2+}	SO_4^{2-}	0.221	3.343/− 37.23	0.025
Na^+	SO_4^{2-}	0.01958	1.113	0.00497
Na^+	OH^-	0.0864	0.253	0.0044
$MgB(OH)_4^+$	SO_4^{2-}	0.7806 (PW)	1.74[a] (PW)	0 (PW)
Pitzer parameters for neutral species and mixing				
Species, *i*	Species, *j*	Species, *k*	θ_{ij} or λ_{ij}	Ψ_{ijk}
$MgSO_4$(aq)	Cl^-		0.32 (PW)	
Mg^{2+}	Na^+	SO_4^{2-}	0.07	− 0.015
Na^+	$MgB(OH)_4^+$		− 0.2975 (PW)	
Equilibrium constants at infinite dilution for dissolution reaction of brucite and dissociation reactions of $MgOH^+$, $MgB(OH)_4^+$ and $MgSO_4$(aq)				
Reactions			$\log_{10} K^\circ$	
$Mg(OH)_2(cr) + 2H^+ \rightleftharpoons Mg^{2+} + 2H_2O(l)$			17.05 ± 0.20 [16]	
$MgOH^+ + H^+ \rightleftharpoons Mg^{2+} + H_2O(l)$			11.8091	
$MgB(OH)_4^+ \rightleftharpoons Mg^{2+} + B(OH)_4^-$			− 1.3993	
$MgSO_4(aq) \rightleftharpoons Mg^{2+} + SO_4^{2-}$			− 2.38 ± 0.08 (PW)	

Unless otherwise noted below, values without annotations are the default values from DATA0.FM1 [31], which is based on Harvie et al. [32] for major ions

[a]This value was not evaluated. It was set to the average value for 1:2 and 2:1 interactions from Choppin et al. [49]

PW present work

The solubilities of brucite as a function of pH_m over a range of ionic strengths predicted by the model with $MgSO_4$(aq) are compared with the experimental data in Figs. 7 and 8 for a more detailed view. It is clear from Figs. 7 and 8 that the model reproduces the experimental data with fair agreement, especially in the high ionic strength range.

In the presence of Mg(II)-bearing solutions, the formation of $MgSO_4$(aq) can influence solubilities of gypsum ($CaSO_4{\cdot}2H_2O$), as total sulfate concentrations are expected to increase when gypsum is dissolved in a Mg-containing medium because of the formation of $MgSO_4$(aq).

$$CaSO_4 \cdot 2H_2O(cr) \rightleftharpoons Ca^{2+} + SO_4^{2-} + 2H_2O(l) \quad (4)$$

Based on solubility data of gypsum in mixtures of NaCl and $MgCl_2$, dominated by NaCl with $MgCl_2$ to 0.325 mol·kg^{-1} and with total ionic strengths up to 5.83 mol·kg^{-1} from Ostruff and Melter [40], the interaction between $MgSO_4$(aq) and Cl^- is evaluated (Table 3). In the work of Ostruff and Melter [40], they measured gypsum solubilities in mixtures of NaCl and $MgCl_2$ at 28 °C. The molality of NaCl ranges from 0.0501 to 5.50 mol·kg^{-1}. The molality of $MgCl_2$ ranges from 0.0100 to 0.325 mol·kg^{-1}. In this

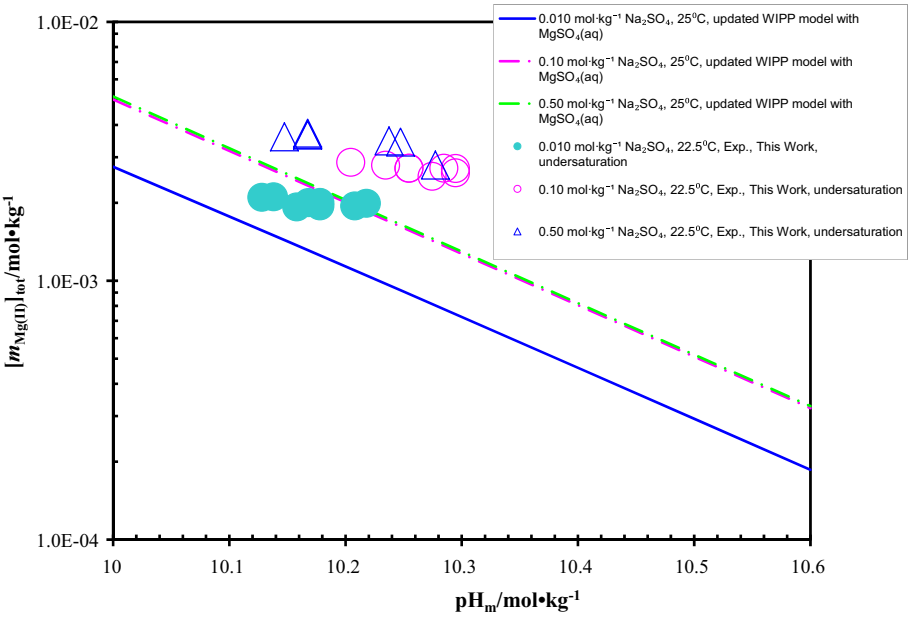

Fig. 7 A plot showing molalities of magnesium in equilibrium with brucite as a function of pH_m in Na_2SO_4 solutions ranging from 0.01 to 0.5 mol·kg^{-1}, in comparison with the predicted values using the model with $MgSO_4$(aq). The predicted values were generated using the database, DATA0.FM2 [47, 48] (see Table 3)

work, the interaction between $MgSO_4$(aq) and Cl^- is modeled based on their experimental data at 28 °C, and other parameters including the solubility constant of gypsum are from the DATA0.FM1 [31]. In Fig. 9, solubilities of gypsum predicted by using the model developed in this study are compared with the experimental data in mixtures of NaCl and $MgCl_2$. Figure 9 shows that the predicted values are in good agreement with the experimental values.

As a validation test, the model predicted solubilities of gypsum in $MgSO_4$ solutions with a wide range of ionic strengths at 25 °C are compared with model-independent experimental solubilities in the same medium at the same temperature (Fig. 10). The model-independent experimental data include Dietriech [41], Harkins and Paine [42], Kolosov [43], Wollmann and Voigt [44], Tanji [45], and Friedel [46]. In the model predicted values, they include those predicted by the model without $MgSO_4$(aq), and those with $MgSO_4$(aq). It is clear from Fig. 10 that these two models have similar accuracy up to an ionic strength of $\sim$ 4 mol·kg^{-1}. However, above an ionic strength of 4 mol·kg^{-1}, the model with $MgSO_4$(aq) is in better agreement with model-independent experimental data than the model without $MgSO_4$(aq) (Fig. 10), independently demonstrating that the incorporation of $MgSO_4$(aq) improves the accuracy of the model.

5 Conclusions

In this study, we conducted long-term solubility measurements on brucite at 22.5 °C in Na_2SO_4 solutions from 0.01 to 1.8 mol·kg^{-1} with 0.001 mol·kg^{-1} H_3BO_3. Based on experimental data, we evaluated a set of Pitzer parameters along with the stability constant

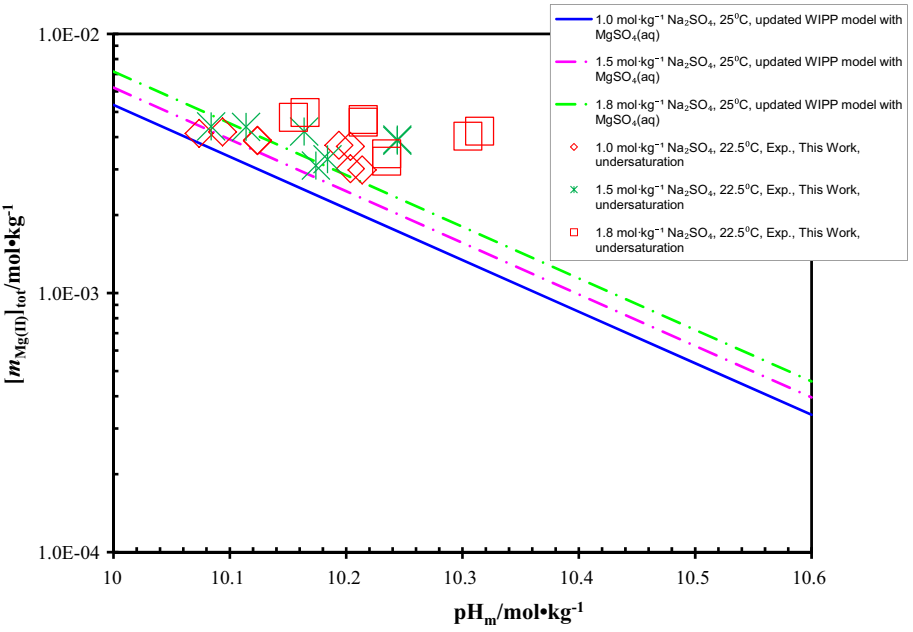

Fig. 8 A plot showing molalities of magnesium in equilibrium with brucite as a function of pH_m in Na_2SO_4 solutions ranging from 1.0 to 1.8 mol·kg^{-1} in comparison with the predicted values using the model with $MgSO_4$(aq). The predicted values were generated using the database, DATA0.FM2 [47, 48] (see Table 3)

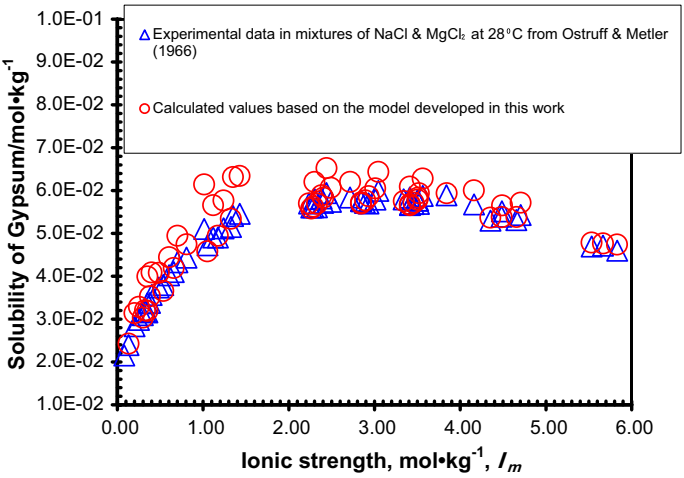

Fig. 9 A plot showing solubilities of gypsum as a function of ionic strength in the mixtures of NaCl and $MgCl_2$

of $MgSO_4$(aq) ($\log_{10} \beta_1^0$) as 2.38 ± 0.08, which is in excellent agreement with the literature values. The model developed in this study can describe not only brucite solubilities in sulfate-bearing solutions, but also gypsum solubilities in mixtures of NaCl and $MgCl_2$ to

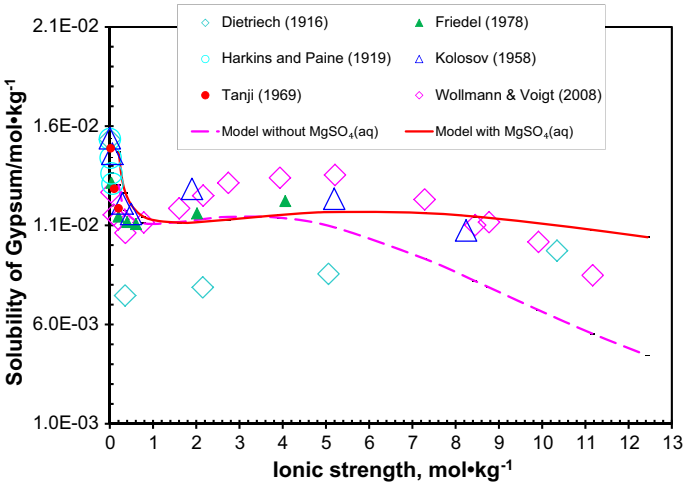

Fig. 10 A plot showing solubilities of gypsum as a function of ionic strength in the $MgSO_4$ solutions. All of the experimental data are model-independent. The predicted values for the model without $MgSO_4$(aq) are generated using the database, DATA0.FM1 [31], whereas those values for the model with $MgSO_4$(aq) are produced employing the database, DATA0.FM2 [47, 48]

$I_m \sim 6$ mol·kg^{-1}, dominated by NaCl with $MgCl_2$ up to ~ 0.4 mol·kg^{-1}, and in $MgSO_4$ solutions up to $I_m \sim 13$ mol·kg^{-1}.

Acknowledgements Sandia National Laboratories is a multi-mission laboratory managed and operated by Sandia Corporation, a wholly owned subsidiary of Lockheed Martin Corporation, for the U.S. Department of Energy's National Nuclear Security Administration under contract DE-AC04-94AL85000. This research is funded by the WIPP programs administered by the Office of Environmental Management (EM) of the U.S. Department of Energy. SAND2017-13513J. The laboratory assistance from Lindsay Day, Diana Goulding, Brittany Hoard, Chase Kicker, Danelle Morrill, Cassandra Marrs, Rachael Roselle, Mathew Stroble, William Sullvan, Kira Vincent, and Yoni Xiong is gratefully acknowledged. The authors are grateful to the three journal reviewers for their insightful and thorough reviews, which have improved the presentation of the article, and to Dr. Magdalena Bendová, the journal editor, for her time and editorial efforts. The authors wish to thank Dr. Earle Waghorne, Editor-in-Chief, for his invitation to the first and senior author to contribute to the special issue of ISSP-17.

References

1. Xiong, Y.-L., Lord, A.C.: Experimental investigations of the reaction path in the MgO–CO_2–H_2O system in solutions with various ionic strengths, and their applications to nuclear waste isolation. Appl. Geochem. **23**, 1634–1659 (2008)
2. Krumhansl, J.L., Panenguth, H.W., Zhang, P.-C., Kelly, J.W., Anderson, H.L., Hardesty, J.O.: Behavior of MgO as a CO_2 scavenger at the Waste Isolation Pilot Plant (WIPP), Carlsbad, New Mexico. Mater. Res. Soc. Symp. Proc. **608**, 155–160 (2000)
3. Schüssler, W., Metz, V., Kienzler, B., Vejmelka, P.: Geochemically based source term assessment for the Asse salt mine: comparison of modeling and experimental results (Abstract). Programs and Abstracts of Materials Research Society Annual Meeting at Boston, MA, p. 713 (2002)
4. Schuessler, W., Kienzler, B., Wilhelm, S., Neck, V., Kim, J.I.: Modeling of near field actinide concentrations in radioactive waste repositories in salt formations: effect of buffer materials. Mater. Res. Soc. Symp. Proc. **663**, 791 (2000)
5. Guerrero, A., Goni, S., Hernandez, M.-S.: Thermodynamic solubility constant of $Ca(OH)_2$ in simulated radioactive sulfate liquid waste. J. Am. Ceram. Soc. **83**, 882 (2000)

6. Moukwa, M.: Characteristics of the attack of cement paste by $MgSO_4$ and $MgCl_2$ from the pore structure measurements. Cem. Concr. Res. **20**, 148–158 (1990)
7. Gollop, R.S., Taylor, H.F.W.: Microstructural and microanalytical studies of sulfate attack. IV. Reactions of a slag cement paste with sodium and magnesium sulfate solutions. Cem. Concr. Res. **26**, 1013–1028 (1996)
8. Santhanam, M., Cohen, M.D., Olek, J.: Mechanism of sulfate attack: a fresh look Part 1: summary of experimental results. Cem. Concr. Res. **32**, 915–921 (2001)
9. Tumidajski, P.J., Chan, G.W.: Durability of high performance concrete in magnesium brine. Cem. Concr. Res. **26**, 557–565 (1996)
10. Battocchi, D., Simoes, A.M., Tallman, D.E., Bierwagen, G.P.: Comparison of testing solutions on the protection of Al-alloys using a Mg-rich primer. Corros. Sci. **48**, 2226–2240 (2006)
11. Yang, L.J., Wei, Y.H., Hou, L.F., Zhang, D.: Corrosion behaviour of die-cast AZ91D magnesium alloy in aqueous sulphate solutions. Corros. Sci. **52**, 345–351 (2010)
12. Tian, Y., Yang, L.J., Li, Y.F., Wei, Y.H., Hou, L.F., Li, Y.G., Murakami, R.I.: Corrosion behaviour of die-cast AZ91D magnesium alloys in sodium sulphate solutions with different pH values. Trans. Nonferrous Met. Soc. China **21**, 912–920 (2011)
13. King, A.D., Kannan, B., Scully, J.R.: Environmental degradation of a Mg-rich primer in selected field and laboratory environments: part 1–without a topcoat. Corrosion **70**, 512–535 (2014)
14. Zeng, R.C., Hu, Y., Guan, S.K., Cui, H.Z., Han, E.H.: Corrosion of magnesium alloy AZ31: the influence of bicarbonate, sulphate, hydrogen phosphate and dihydrogen phosphate ions in saline solution. Corros. Sci. **86**, 171–182 (2014)
15. Lin, J., Battocchi, D., Bierwagen, G.: Degradation of magnesium rich primers over AA2024-T3 during constant immersion in different solutions. Corrosion **73**, 408–416 (2017)
16. Xiong, Y.-L.: Thermodynamic properties of brucite determined by solubility studies and their significance to nuclear waste isolation. Aquat. Geochem. **14**, 223–238 (2008)
17. Wood, S.A., Palmer, D.A., Wesolowski, D.J., Bénézeth, P.: The aqueous geochemistry of the rare earth elements and yttrium. Part XI. The solubility of $Nd(OH)_3$ and hydrolysis of Nd^{3+} from 30 to 290 °C at saturated water vapor pressure with in-situ pHm measurement. In: Hellmann, R., Wood, S.A. (eds.) Special Publication 7, pp. 229–256. The Geochemical Society (2002)
18. Rai, D., Felmy, A.R., Juracich, S.I., Rao, F.F.: Estimating the Hydrogen Ion Concentration in Concentrated NaCl and Na_2SO_4 Electrolytes. SAND94-1949. Sandia National Laboratories, Albuquerque, NM (1995)
19. Roselle, G.: Determination of pC_{H+} Correction Factors in Brines. Work Carried Out under the Analysis Plan for Determination of pC_{H+} Correction Factors in Brines, AP157, Rev 0. Sandia National Laboratories, Carlsbad, NM (2011)
20. Xiong, Y.-L., Deng, H.-R., Nemer, M., Johnsen, S.: Experimental determination of the solubility constant for magnesium chloride hydroxide hydrate ($Mg_3Cl(OH)_5{\cdot}4H_2O$, phase 5) at room temperature, and its importance to nuclear waste isolation in geological repositories in salt formations. Geochim. Cosmochim. Acta **74**, 4605–46011 (2010)
21. Leito, I., Strauss, L., Koort, E., Pihl, V.: Estimation of uncertainty in routine pH measurement. Accred. Qual. Assur. **7**, 242–249 (2002)
22. McGee, K.A., Hostetler, P.B.: Activity-product constants of brucite from 10 to 90 °C. J. Res. US Geol. Surv. **5**, 227–233 (1977)
23. Wolery, T.J., Xiong, Y.-L., Long, J.: Verification and Validation Plan/Validation Document for EQ3/6 Version 8.0a for Actinide Chemistry, Document Version 8.10. Carlsbad, NM: Sandia National laboratories. ERMS 550239 (2010)
24. Xiong, Y.-L.: WIPP Verification and Validation Plan/Validation Document for EQ3/6 Version 8.0a for Actinide Chemistry, Revision 1, Document Version 8.20. Supersedes ERMS 550239. Carlsbad, NM. Sandia National Laboratories. ERMS 555358 (2011)
25. Xiong, Y.-L., Kirkes, L., Westfall, T.: Experimental determination of solubilities of sodium tetraborate (borax) in NaCl solutions, and a thermodynamic model for the Na–$B(OH)_3$–Cl–SO_4 system to high ionic strengths at 25 °C. Am. Mineral. **98**, 2030–2036 (2013)
26. Xiong, Y.-L., Kirkes, L., Westfall, T., Roselle, R.: Experimental determination of solubilities of lead oxalate (PbC_2O_4(cr)) in a NaCl medium to high ionic strengths, and the importance of lead oxalate in low temperature environments. Chem. Geol. **342**, 128–137 (2013)
27. Xiong, Y.-L.: Experimental determination of lead carbonate solubility at high ionic strengths: a Pitzer model description. Monatsh. Chem. **146**, 1433–1443 (2015)
28. Xiong, Y.-L.: An aqueous thermodynamic model for solubility of potassium ferrate in alkaline solutions to high ionic strengths at 283.15 to 333.15 K. J. Solution Chem. **42**, 1393–1403 (2013)

29. Xiong, Y.-L.: A thermodynamic model for silica and aluminum in alkaline solutions with high ionic strength at elevated temperatures up to 100 °C: applications to zeolites. Am. Mineral. **98**, 141–153 (2013)
30. Xiong, Y.-L.: A Pitzer model for the Na–$Al(OH)_4$–Cl–OH system and solubility of boehmite (AlOOH) to high ionic strength and to 250 °C. Chem. Geol. **373**, 37–49 (2014)
31. Xiong, Y.-L.: Release of EQ3/6 Database DATA0.FM1. Carlsbad, NM: Sandia National Laboratories. ERMS 555152 (2011)
32. Harvie, C.E., Moller, N., Weare, J.H.: The prediction of mineral solubilities in natural waters: The Na–K–Mg–Ca–H–Cl–SO_4–OH–HCO_3–CO_3–CO_2–H_2O system to high ionic strengths at 25 °C. Geochim. Cosmochim. Acta **48**, 723–751 (1984)
33. Daly, F.P., Brown, C.W., Kester, D.R.: Sodium and magnesium sulfate ion pairing: evidence from Raman spectroscopy. J. Phys. Chem. **76**, 3664–3668 (1972)
34. Katayama, S.: Conductometric determination of ion-association constants for magnesium and nickel sulfates in aqueous solutions at various temperatures between 0 and 45 °C. Bull. Chem. Soc. Jpn **46**, 106–109 (1973)
35. Elgquist, B., Wedborg, M.: Stability of ion pairs from gypsum solubility degree of ion pair formation between the major constituents of seawater. Mar. Chem. **3**, 215–225 (1975)
36. Rudolph, W.W., Irmer, G., Hefter, G.: Raman spectroscopic investigation of speciation in $MgSO_4$(aq). Phys. Chem. Chem. Phys. **5**, 5253–5261 (2003)
37. Nair, V.S.K., Nancollas, G.H.: Thermodynamics of ion association. Part IV. Magnesium and zinc sulphates. J. Chem. Soc. 3706–3710 (1958)
38. Kester, D.R.: Ph.D. Thesis, Oregon State University, Corvallis (1969)
39. Kratsis, S., Hefter, G., May, P.: Potentiometric study of the association of magnesium and sulfate ions at 25 °C in high ionic strength media. J. Solution Chem. **30**, 19–29 (2001)
40. Ostroff, A.G., Metler, A.V.: Solubility of calcium sulfate dihydrate in the system NaCl–$MgCl_2$–H_2O from 28 °C to 70 °C. J. Chem. Eng. Data **11**, 346–350 (1966)
41. Dietriech, H.G.: Kaminer Handbuch der Balneologie **1**, 205 (1916)
42. Harkins, W.D., Paine, H.M.: Intermediate and complex ions. V. The solubility product and activity of the ions in bi-bivalent salts. J. Am. Chem. Soc. **41**, 1155–1168 (1919)
43. Kolosov, A.S.: Isotherms of the system $MgSO_4$–$CaSO_4$–H_2O at 25 °C. Trudy Khim.-Met. Inst., Akad. Nauk S.S.S.R., Zapadno-Sibir. Filial **35**, 29–38 (1958)
44. Wollmann, G., Voigt, W.: Solubility of gypsum in MSO_4 solutions (M = Mg, Mn Co, Ni, Cu, Zn) at 298.15 K and 313.15 K. J. Chem. Eng. Data **53**, 1375–1380 (2008)
45. Tanji, K.K.: Solubility of gypsum in aqueous electrolytes as affected by ion association and ionic strengths up to 0.15 M and at 25 deg. Environ. Sci. Technol. **3**, 656–661 (1969)
46. Friedel, B.: Gypsum solubilities in aqueous systems containing NaCl, $MgCl_2$, Na_2SO_4, and $MgSO_4$. Z. Pflanzenernahrung und Bodenkunde **141**, 337–346 (1978)
47. Domski, P.S.: Memo AP-173, EQ3/6 Database Update: DATA0.FM2. Carlsbad, NM, Sandia National Laboratories, ERMS 564914 (2015)
48. Xiong, Y.-L., Domski, P.S.: Updating the WIPP Thermodynamic Database, Revision 1, Supersedes ERMS 565730. Carlsbad, NM: Sandia National Laboratories. ERMS 566047 (2016)
49. Choppin, G.R., Bond, A.H., Borkowski, M., Bronikowski, M.G., Chen, J.-F., Lis, S., Mizera, J., Pokrovsky, O.S., Wall, N.A., Xia, Y.-X., Moore, R.C.: Waste isolation pilot plant actinide source term test program: solubility studies and development of modeling parameters. Sandia National Laboratories Report. SAND99-0943 (2001)